Journal of Power Sources 253 (2014) 1–8

Contents lists available at ScienceDirect

Journal of Power Sources

journal homepage: www.elsevier.com/locate/jpowsour

Fabrication of PtCu and PtNiCu multi-nanorods with enhanced catalytic oxygen reduction activities

Licheng Liu [a], Gabor Samjeské [a], Shinobu Takao [a], Kensaku Nagasawa [a], Yasuhiro Iwasawa [a,b,*]

[a] Innovation Research Center for Fuel Cells, The University of Electro-Communications, Choufugaoka, Chofu, Tokyo 182-8585, Japan
[b] Department of Engineering Science, Graduate School of Information Engineering Science, The University of Electro-Communications, Choufugaoka, Chofu, Tokyo 182-8585, Japan

HIGHLIGHTS

- Metallic PtCu and PtNiCu multi-nanorods with 5 nm diameter and 10 nm length were fabricated by a polyol reduction method.
- Copper precursor dependency on the fabrication of both PtCu and PtNiCu nanorods was observed.
- The multi-nanorods were successfully synthesized with $CuCl_2$, $Cu(CH_3COO)_2$ and $CuSO_4$ as Cu precursors but not with $Cu(NO_3)_2$.
- The multi-nanorods showed 2–5 times enhanced electrocatalytic activities with good stability for ORR than a Pt/C catalyst.

ARTICLE INFO

Article history:
Received 17 October 2013
Received in revised form
25 November 2013
Accepted 7 December 2013
Available online 14 December 2013

Keywords:
Metal multi-nanorods fabrication
Pt alloy nanorods
PtCu
PtNiCu
Electrocatalysts
Oxygen reduction reaction

ABSTRACT

1-D metallic nanomaterials have received much attention from the viewpoints of material functions of shape-controlled nanocrystals and applications to a variety of technologies. Metallic PtCu and PtNiCu multi-nanorods with diameter of about 5 nm and average length of around 10 nm were fabricated by polyol reduction method and characterized by TEM/EDS, XRD, XRF and electrochemical techniques. The multi-nanorods were successfully synthesized with $CuCl_2$, $Cu(CH_3COO)_2$ and $CuSO_4$ as Cu precursors but not with $Cu(NO_3)_2$, showing precursor dependency on the nanorod fabrication. The fcc alloy-crystal structures were observed with these multi-nanorods, which showed much more enhanced electrocatalytic activities with good stability for oxygen reduction reaction (ORR) than a conventional Pt/C catalyst. The results demonstrate that Pt-based multimetallic nanocrystals are promising candidates for cathode catalysts to develop next-generation polymer electrolyte fuel cells.

1. Introduction

Shape-controlled synthesis of metallic nanocrystals has received much interest in modern material chemistry as well as potential applications to a variety of technologies because the intrinsic property and functions of most nanomaterials strongly depends on the nano-shape and morphology [1–5]. Among various fabricated shapes, monometallic and multimetallic 1-D nano-materials, such as nanowires [6–9], nanobars [10], nanorods [11–14], and nanodendrites [15–18] have attracted much attention due to their unique photoelectric, magnetic and catalytic properties. Pt-based multimetallic nanocrystals have been applied to many technologies such as catalysis, electronics and photonics [19,20] and particularly polymer electrolyte fuel cells (PEFC), where they have been regarded as potential candidates for cathode catalysts for oxygen reduction reaction (ORR) [21–23]. Increasing ORR activity, improving durability, decreasing costs and high-volume production of cathode catalysts are still prerequisite for development of next-generation PEFCs [24].

The Pt mono- or bimetallic nano-composites with various shapes and morphologies, such as Pt nanocubes [25,26], Pd–Pt nanodentrites [15], octahedral Pt–Ni [27–29], have been synthesized and demonstrated to be highly active for ORR. Among them, 1-D Pt and Pt-alloy nanocrystals exhibited high ORR activities due

* Corresponding author. Innovation Research Center for Fuel Cells, The University of Electro-Communications, Choufugaoka, Chofu, Tokyo 182-8585, Japan. Fax: +81 42 443 5483.
E-mail addresses: iwasawa@pc.uec.ac.jp, iwasawa@chem.s.u-tokyo.ac.jp (Y. Iwasawa).

0378-7753/$ – see front matter © 2013 Elsevier B.V. All rights reserved.
http://dx.doi.org/10.1016/j.jpowsour.2013.12.028

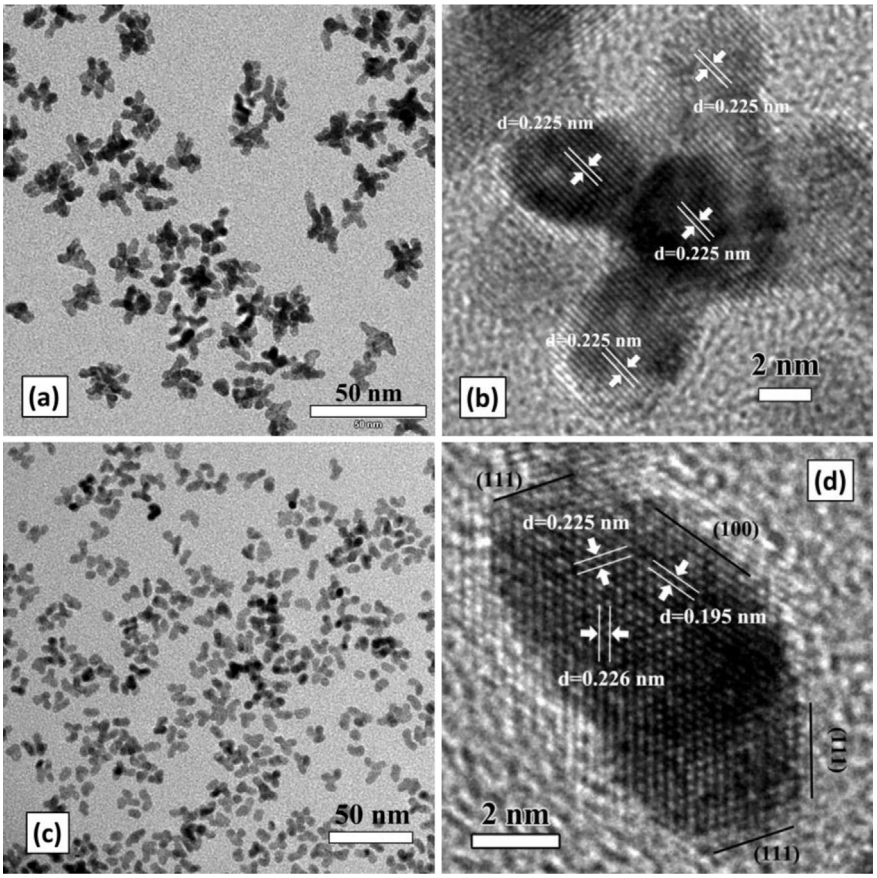

Fig. 1. TEM images of PtCu and PtNiCu multi-rods (a, c) and the corresponding high-resolution STEM images (b, d).

to their unique structures and electronic confinement effect. Sun et al. [30] synthesized star-like Pt nanowires with ≈4 nm diameter and ≈15 nm length by formic acid reduction method, which showed 1.5 times higher mass activity and 3 times higher specific activity compared to a commercial Pt/C catalyst. Koenigsmann et al. [31] reported the synthesis and electrocatalytic performance of ultrathin Pt nanowires with less than 2 nm diameter and up to 100 nm length, which displayed 7 times larger specific activity than spherical Pt nanoparticles. Zhang et al. [9] demonstrated that the mass activity of ultra-thin PtFe-nanowires with a diameter of 2–3 nm was 2 times larger than a standard Pt/C.

Herein, we report the synthesis of wormlike PtCu and PtNiCu multi-nanorods on carbon support by an ethylene glycol (EG) reduction method with PVP as a capping agent. The multi-nanorods with the dimensions of 4–5 nm diameter and 6–16 nm length exhibited 2–5 times larger ORR activities than a Pt/C (TKK, TEC10E60TPM).

2. Experimental

2.1. Syntheses of nanocrystals and carbon-supported nanocrystals

2.1.1. Chemicals

Chloroplatinic acid hexahydrate ($H_2PtCl_6 \cdot 6H_2O$, Sigma–Aldrich), copper chloride ($CuCl_2$, Wako), copper sulfate pentahydrate ($CuSO_4 \cdot 5H_2O$, Wako), copper acetate ($Cu(CH_3COO)_2$, Wako), copper nitrate ($Cu(NO_3)_2$, Wako), nickel chloride ($NiCl_2$, Wako), ethylene glycol (Wako), and polyvinyl pyrrolidone (PVP-k30, Wako) were commercially obtained. Solvents of analytical grade, such as ethanol, hexane and acetone were used without further purification.

2.1.2. Synthesis of PtCu multi-nanorods

A typical synthesis process was described as follows. 113 mg PVP was added to 11 ml EG. The mixture was heated at 373 K and kept for 30 min under stirring in a N_2 flow. Then 106 mg of $H_2PtCl_6 \cdot 6H_2O$ and 9.2 mg $CuCl_2$ were dissolved into above EG solution under stirring. The resultant solution was heated to 438 K in an oil bath under stirring, at which temperature it was kept for 1 h. After cooling down, the produced nanoparticles were precipitated by adding acetone and separated by centrifugation and washed by ethanol and *n*-hexane. The colloidal nanoparticles were suspended and stored in 10 ml of ethanol. For synthesis from other copper precursors, the amount of copper precursors was controlled to ensure the feeding Pt/Cu molar ratio is 3/1.

2.1.3. Synthesis of PtNiCu multi-nanorods

The synthesis procedures were similar to the above procedures except the use of 4.4 mg $NiCl_2$ and 4.6 mg $CuCl_2$ instead of 9.2 mg $CuCl_2$. For synthesis from other copper precursors, the amounts of nickel and copper salt were regulated to make the feeding Pt/Ni/Cu molar ratio to be 3/0.5/0.5.

2.1.4. Preparation of carbon-supported nanorod catalysts

The as-synthesized nanorods were dispersed in ethanol, to which 60 mg of carbon (Vulcan XC-72) was added. The resultant suspension was placed in an ultrasonic bath for 1 h and then stirred overnight. The obtained carbon-supported catalysts were collected by centrifugation and dried in air. For removing PVP residuals in the samples, the catalysts were calcined at 473 K for 2 h in 20% O_2/N_2 gas flow.

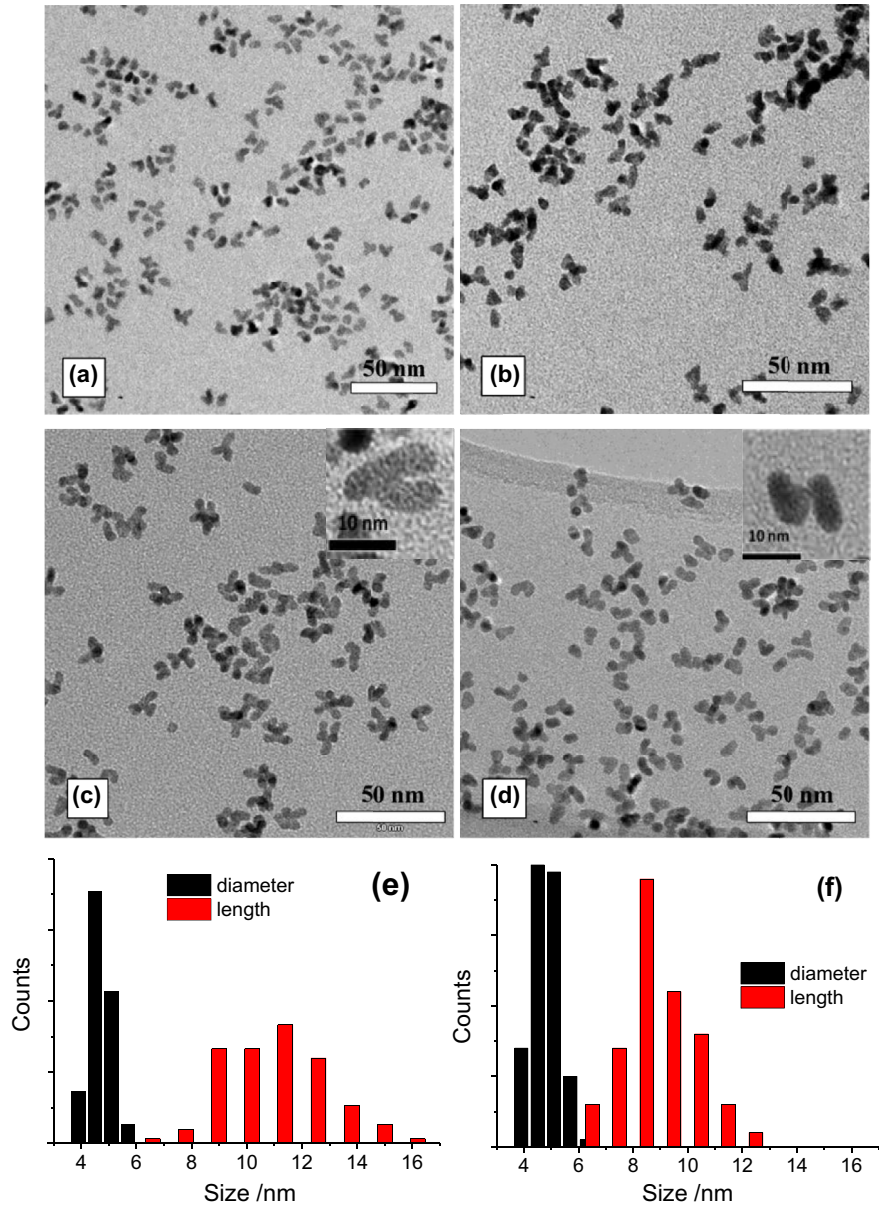

Fig. 2. TEM images of PtCu multi-rods fabricated from H_2PtCl_6 and different Cu precursor salts of (a) $Cu(CH_3COO)_2$ and (b) $CuSO_4$, and PtNiCu multi-rods fabricated from H_2PtCl_6, $NiCl_2$ and different Cu precursor salts of (c) $CuCl_2$ and (d) $CuSO_4$. Diameter and length distributions of PtNiCu nanorods fabricated from $CuCl_2$ (e) and $CuSO_4$ (f).

2.2. Characterization and instruments

Transmission electron microscopic (TEM) images were measured on JEOL JEM-2010 and JEM-2100F at an accelerating voltage of 200 kV. After diluting the ethanol suspension containing the metal nanorods with additional ethanol and by ultrasonic treatment, the solution was applied onto copper grids covered with carbon film and dried in vacuum before inserting into the main chamber of JEM-2010 TEM. The carbon-supported powder samples were also dispersed in ethanol ultrasonically before applying onto copper grids.

X-ray diffraction (XRD) patterns were recorded on a Rigaku Ultima III diffractometer with Cu Kα radiation ($\lambda = 0.154178$) at 40 kV and 40 mA. The scanning angle (2θ) ranged from 20° to 90° at a scanning rate of 5°/min. The XRD data were analyzed with MDI Jade 6.0 software.

X-ray fluorescence (XRF) was measured on a Rigaku ZSX Primus II X-ray fluorescence spectrometer with a Rh-anode X-ray generator. The catalysts powder were put in sample chamber and measured by 10 nm diameter in vacuum.

Electrochemical measurements of the synthesized catalysts were performed using an Autolab potentiostat/galvanostat in a standard three-electrode configuration with a reversible hydrogen electrode (RHE) as reference and a platinum foil as counter electrode at room temperature. A glassy carbon (GC) disk electrode (PINE instruments) with a diameter of 5 mm and a geometric area of 0.1963 cm^2 was polished with 0.05 μm alumina before each experiment, and used as a working electrode and a substrate for electrocatalyst film. The thin film catalyst layer on the GC electrode was prepared as follows. A mixture of 12.5 mg of electrocatalyst, 18 ml of Millipore water and 2 ml of Nafion solution (0.5 wt%) was ultrasonicated for 20 min to obtain a well-dispersed ink. The

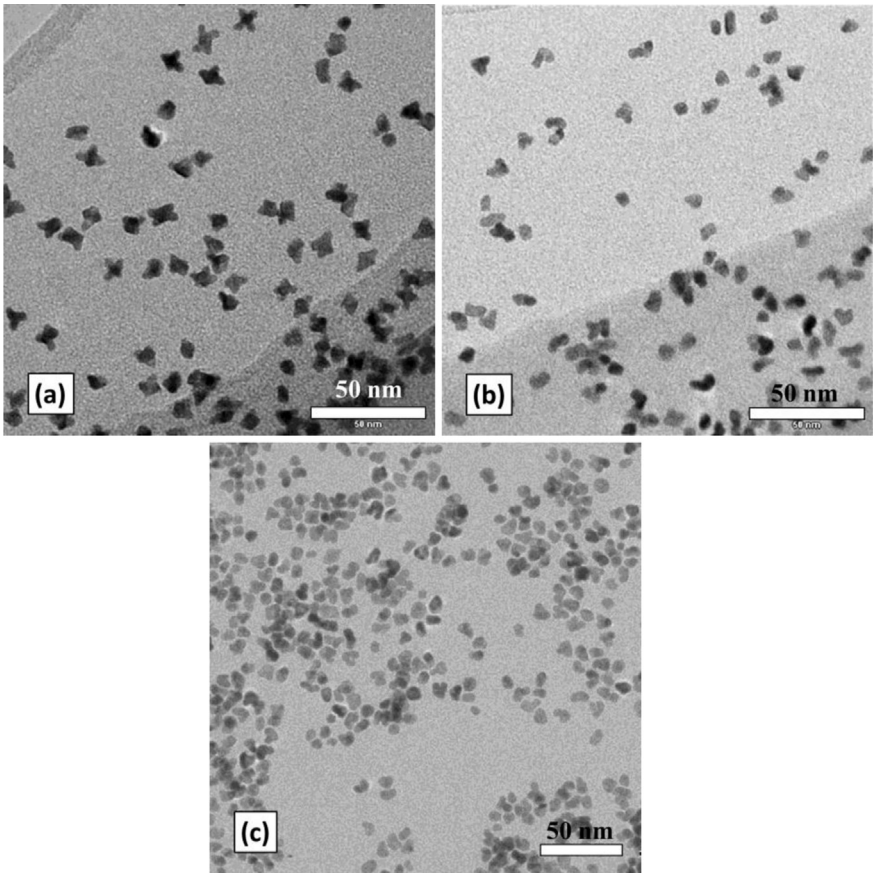

Fig. 3. TEM images of PtNi (a), PtCu (b) and PtNiCu (c) nanoparticles fabricated from precursor salts of H_2PtCl_6, $NiCl_2$ and/or $Cu(NO_3)_2$.

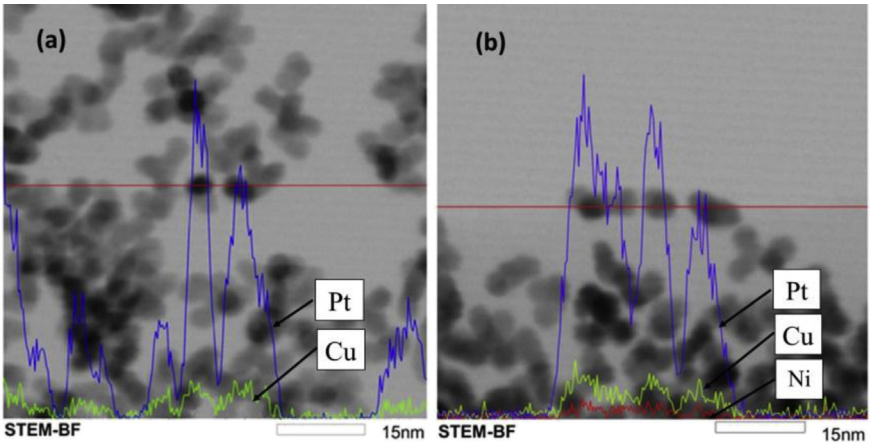

Fig. 4. EDS line analysis of PtCu (a) and PtNiCu (b) multi-nanorods.

catalyst ink of 20 μl was then quantitatively put on the GC electrode by using a micropipette and dried in vacuum to obtain a catalyst thin film. The amount of catalyst ink was regulated to be a metal loading of 25.5 μg cm^{-2} for all catalysts. All electrochemical experiments were conducted by using a 0.1 M $HClO_4$ (Merck) solution and Milipore-Q™ water at 25 °C. The cyclic voltammograms (CV) were recorded between the potential limits of 0.05 V and 1.2 V vs. RHE at a sweep rate of 50 mV s^{-1} and under continuous high-purity nitrogen purging. The ORR activities were examined by linear sweep voltammetry (LSV) by scanning from 0.05 V to 1.0 V vs RHE in the anodic potential sweep direction and at a scan rate of 10 mV s^{-1} in the electrolyte saturated with high-purity oxygen by using a MSR rotator from PINE instruments at a rotation speed of 1600 rpm. The durability test was investigated by repeated CV scanning cycles up to 500 cycles between 0.05 V and 1.2 V vs. RHE at a sweep rate of 50 mV s^{-1}.

3. Results and discussion

Bimetallic PtCu multi-nanorods were at first fabricated by using H_2PtCl_6 and $CuCl_2$ as metal sources. The as-synthesized PtCu nanorods possessed the dimension of about 5 nm diameter and 6–

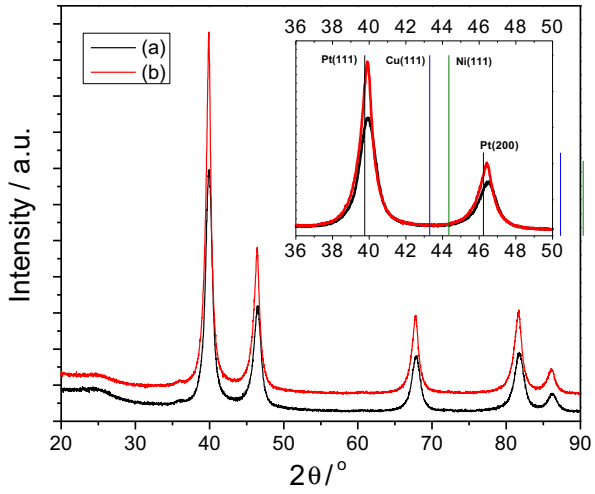

Fig. 5. XRD patterns of carbon-supported PtCu (a) and PtNiCu (b) multi-nanorods.

12 nm length as shown Fig. 1(a). The nanorod shape was dominant in the sample and almost neither spherical nanoparticles nor other shapes were observed. It is to be noted that the PtCu nanorods assemble together to make a nanodendrites-like structure with branches. Crystal fringes of high definition are observed in the STEM image of PtCu nanorods in Fig 1(b). The lattice spacings were estimated to be 0.225 nm, which is a little smaller than Pt (111) spacing (0.227 nm) and referred to (111) crystal plane (0.225 nm) of PtCu alloy [30].

Ternary metallic PtNiCu multi-nanorods were also synthesized by the ethylene glycol (EG) reduction method with PVP using $NiCl_2$ and $Cu(CH_3COO)_2$ as Ni and Cu precursors, respectively, as shown in Fig. 1(c). The average diameter was around 5.0 nm, while the average length was 10.3 nm. The crystal fringe and atomic stacking are clearly observed with the high-resolution STEM image of a selected nanorod in Fig. 1(d), where the (111) and (100) crystal planes can be differentiated in the different orientations with lattice spacings of 0.225/0.226 nm and 0.195 nm [32], of which the exposed surfaces of the fabricated nanorods are composed.

PtCu nanorods were also fabricated by using $Cu(CH_3COO)_2$ or $CuSO_4$ instead of $CuCl_2$ as copper precursors (Fig. 2(a) and (b)). The three different Cu precursors showed no definite effect on the morphology of PtCu nanorods. Similar results were also observed with the synthesis of PtNiCu nanorods. Besides $Cu(CH_3COO)_2$ precursor, PtNiCu nanorods were also successfully fabricated from $CuCl_2$ and $CuSO_4$ precursors, respectively (Fig. 2(c) and (d)). The diameters and lengths of the PtNiCu nanorods fabricated from $CuCl_2$ and $CuSO_4$ by estimated from about 200 nanoparticles as representative samples are shown in Fig. 2(e) and (f). The PtNiCu nanorods showed the diameter around 5.0 nm, and the average lengths varied in the following order for the Cu precursors, 9.0 nm ($CuSO_4$) < 10.3 nm ($Cu(CH_3COO)_2$) < 11.2 nm ($CuCl_2$).

However, our further investigation on the PtCu and PtNiCu nanocrystals fabricated from $Cu(NO_3)_2$ precursor showed that the percentage of nanorods in the total number of nanocrystals decreased dramatically compared with samples synthesized from previous copper precursors, as shown in Fig. 3(a) and (b), where most products were irregular nanoparticles with different shapes and sizes. So the anions in the Cu precursor salts, CH_3COO^-, SO_4^{2-}, Cl^- and NO^{3-}, also influence the formation and growth of PtCu and PtNiCu multi-nanorods through adsorption on the nanocrystal surface. Bimetallic PtNi nanocrystals were also synthesized by using $NiCl_2$ precursor under the similar synthesis conditions, but only conventional nanoparticles with an average size around 10 nm were observed as imaged in Fig. 3(a). This implies that copper may be essential for the multi-nanorods generation.

For elucidating the structure and composition of the as-synthesized PtCu and PtNiCu nanorods, the represented samples in Fig. 1 were characterized by EDS line analysis as shown in Fig. 4. In the PtCu nanorods, Pt and Cu distributed with similar compositions in each single nanoparticle. Similarly, nearly uniform distribution of Pt, Ni and Cu elements was also found for PtNiCu nanorods. The surface composition is suggested to be similar to the bulk composition by the EDS line analysis (Fig. 4), where neither serious surface segregation nor core–shell structure were observed. The alloy structure was further confirmed by XRD for the multi-nanorods supported on Vulcan XC-72 carbon (Fig. 5). The XRD patterns showed the typical fcc crystal structure, and PtCu and PtNiCu alloyings were suggested by small shifts of the diffraction peaks to higher angles due to lattice contraction. The d_{111} spacings of PtCu and PtNiCu calculated from the (111) diffraction peaks were 0.2253 and 0.2254 nm, respectively, corresponding to the STEM images in Fig. 1. The element compositions of PtCu and PtNiCu nanorods were estimated to be $Pt_3Cu_{0.46}$ and $Pt_3Ni_{0.13}Cu_{0.42}$ from the EDS line profile areas (Fig. 4). Their element compositions were also estimated as $Pt_3Cu_{0.65}$ and $Pt_3Ni_{0.18}Cu_{0.41}$, respectively by X-ray fluorescence (XRF) (Fig. 6). The Cu and Ni concentrations determined by both methods were lower than the theoretical values of Pt_3Cu_1 and $Pt_3Ni_{0.5}Cu_{0.5}$. By assuming perfectly random alloys, the d_{111} spacings of PtCu and PtNiCu were calculated to be 0.2242 and 0.2236 nm, respectively through the Vegard's law from the compositions of $Pt_3Cu_{0.46}$ and $Pt_3Ni_{0.13}Cu_{0.42}$ determined by EDS line

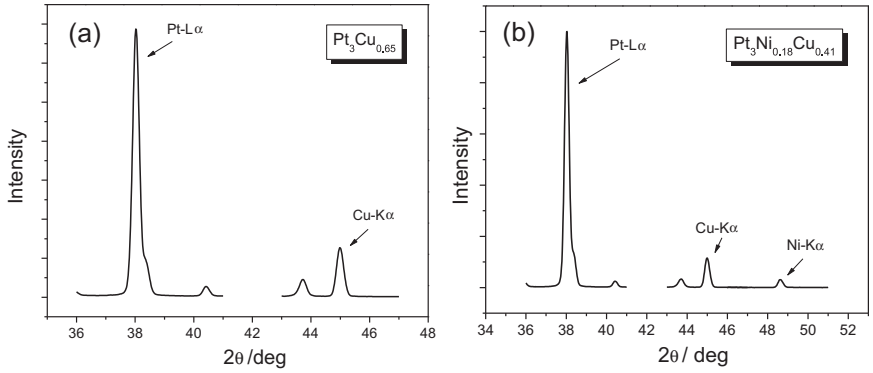

Fig. 6. XRF results of carbon-supported PtCu (a) and PtNiCu (b) multi-nanorods.

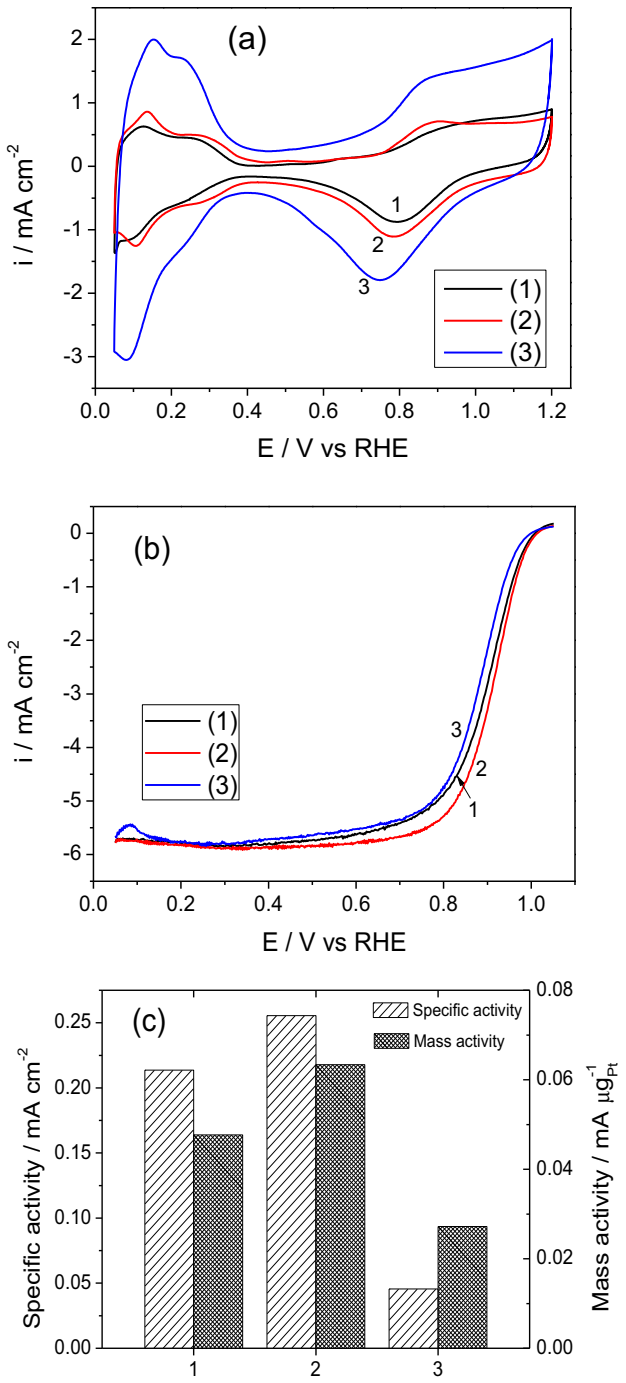

Fig. 7. Cyclic voltammetry curves (a), ORR polarization curves (b) and mass/specific activities at 0.93 V vs RHE (c) of PtCu multi-rods/C (1), PtNiCu multi-rods/C (2) and Pt/C (TEC10E60TPM) (3).

profile analysis. These values are smaller than the experimentally estimated values from the XRD (0.2253 and 0.2254 nm) and STEM (0.225 and 0.225/0.226 nm), suggesting that the part of Ni and Cu atoms stayed out of the alloy lattices by leaching.

As well known, the electrochemical reactivity series of Pt, Cu and Ni metals is consistent to the order of standard electrode potentials, Ni > Cu > Pt. It means that Pt^{4+} can be reduced by Ni and Cu ($Pt^{4+} + 2M \rightarrow Pt + 2M^{2+}$) and Cu^{2+} can be reduced by Ni ($Cu^{2+} + Ni \rightarrow Cu + Ni^{2+}$). These reactions may occur during the ethylene glycol reduction process, which decreases the reduction efficiency of Ni and Cu and reduces their amounts involved in the final Pt-based alloy products. At the initial stage of the reduction process, small crystal nuclei of Pt as a main component are regarded to form exposing different crystal planes such as (110), (100), and (111) with different surface energies [33]. Cu^{2+} ions are reduced by ethylene glycol to Cu metal atoms and deposited on the surface of Pt nuclei. And the Cu metal atoms can promote Pt reduction and crystallization by the galvanic displacement reaction above mentioned [34]. This will lead to different growing rates on different crystal planes and thus preferential growth of nanocrystals on a specific plane, resulting in production of multi-nanorods. The lack of this effect for Ni is possibly attributed to improper rates of the reduction and reaction. Galvanic replacement reaction has been widely used in shape and morphology control in synthesis of metal nano-structures [35–39]. Regarding the anion effect on the Cu deposition, the adsorption of NO_3^- on Pt may be weaker than the other anions and Cu can be deposited on every plane freely, which results in multi-directional growth and irregular morphology.

The electrochemical properties and ORR activities of carbon supported PtCu and PtNiCu multi-nanorods were investigated and compared with those of Pt/C (TEC10E60TPM). The multi-nanorod structures were mostly preserved after supporting PtNiCu and PtCu multi-nanorods on carbon (TEM, not shown). However, the outermost surface composition of carbon-supported PtCu and PtNiCu samples after CV cycles in 0.1 M $HClO_4$ may vary from the bulk composition to form Pt-enriched surfaces due to leaching of Cu and Ni, and further study is needed to decide the Pt-enriched surface composition. The multi-nanorods/C and nanoparticles/C

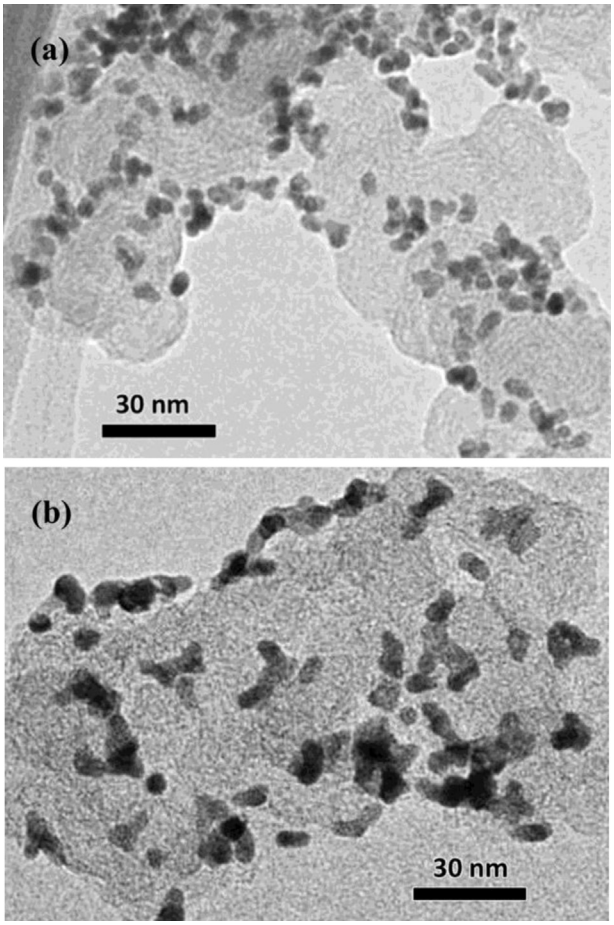

Fig. 8. TEM images of carbon-supported PtNiCu multi-nanorods (from $Cu(CH_3COO)_2$). (a) Fresh; (b) after long-term CV in 0.1 M $HClO_4$.

catalysts exhibited lower current densities than the Pt/C catalyst as seen in the cyclic voltammetry (CV) curves measured in 0.1 M $HClO_4$ (Fig. 7(a)). The electrochemical surface areas (ECSA) for PtCu multi-nanorods/C, PtNiCu multi-nanorods/C and Pt/C catalysts were calculated from the CV hydrogen region to be 22.3, 24.8 and 59.7 $m^2\ g^{-1}$, respectively. The ORR polarization curves of the PtCu/C and PtNiCu/C catalysts increased in the kinetic region (e.g., around 0.9 V) in comparison with the Pt/C catalyst in Fig. 7(b). The calculated mass activities per g_{Pt} (mA μg_{Pt}^{-1}) and specific activities per ECSA (mA cm^{-2}) at 0.93 V vs RHE for the three catalysts are shown in Fig. 7(c), which revealed the PtCu/C and PtNiCu/C catalysts were more active than the Pt/C catalyst. We have chosen the potential of 0.93 V rather than 0.9 V for comparison of the ORR activities to minimize inaccuracy of the mass-transport correction on the calculation of kinetic currents based on the Koutecky–Levich equation. Such a selection of the slightly higher potential has also been reported in the literature [3,40]. The activities of the multi-nanorods/C catalysts at 0.93 V are also higher than a Pt/C catalyst with a similar Pt particle size around 5 nm reported in the literature [40]. Particularly, the specific activity and mass activity of the PtNiCu multi-nanorods/C were found to be about 5 times and 2 times higher than those of the Pt/C (TEC10E60TPM), respectively (Fig. 7(c)).

In addition, the PtNiCu multi-nanorods catalysts also showed good stability in long-term CV scanning. After 500 load cycles between 0.05 V and 1.2 V vs RHE in 0.1 M $HClO_4$, a part of the PtNiCu multi-nanorods on carbon was observed to grow to longer nanorods than the fresh ones (Fig. 8), but there was almost no significant change in the CV curve shape for the PtNiCu/C (Fig. 9(a)). The hydrogen adsorption/desorption peaks showed a little shrinking, but the reduction peak for O adsorbed species around 0.8 V was almost repeatable after the 500 load cycles. In the ORR polarization curves (Fig. 9(b)) only a little drop was observed.

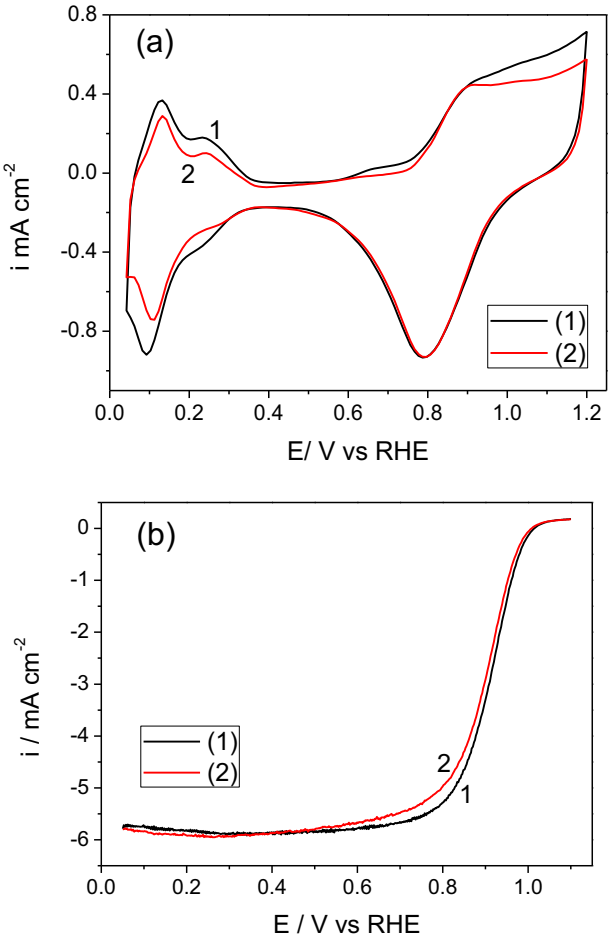

Fig. 9. Cyclic voltammetry (a) and ORR polarization curves (b) of fresh (1) and 500 load cycles-loaded (2) PtNiCu multi-rods/C.

The enhanced ORR activity of the multi-nanorod catalysts can be attributed to the alloy structure, where the surface roughness due to leaching out of Ni or Cu atoms, compressive strain effect (bond distance), ligand effect, and downward Pt d-band center may contribute to the enhancement of ORR kinetics [22]. On the other hand, the presence of edge sites with low coordination atoms at nanoparticle surfaces has been demonstrated to lead to low specific activity of the nanoparticles due to the much stronger oxygen binding energy at these sites [40]. The nanorod structure may reduce the edge sites with less activity and provide side-face atoms with higher coordination in comparison with a spherical nanostructure with the similar size (diameter). This may be another reason for improving activity of the nanorod catalysts [31]. Further investigation is needed for characterizing active surface structures of the multi-nanorods to promote the ORR performance.

4. Conclusions

The PtCu and PtNiCu multi-nanorods were successfully synthesized with a variety of metal precursors by an ethylene glycol reduction method. Both copper and counter-anions affected the nanorods fabrication. Co-reduction of copper ions in the synthesis was found to be essential for the conformation of nanorods. Copper precursors such as $CuCl_2$, $Cu(CH_3COO)_2$ and $CuSO_4$ were successfully applied to the fabrication of PtCu and PtNiCu multi-nanorods, which possess the fcc alloy crystal structures. However, $Cu(NO_3)_2$ precursor did not lead to assembling of the PtCu and PtNiCu multi-nanorods. The 2–5 times enhanced ORR activity (mass and specific) with good stability was achieved with the ternary multi-nanorods/C catalyst. The ORR kinetics of the multi-nanorod catalysts may depend on the alloy structure with Pt-enriched surface roughness, compressive strain effect, ligand effect and downward Pt d-band center. To make PEFC automobiles practical realization and spread, useful fabrication of new catalysts for increasing ORR activity and improving durability is still demanded. This study provides promising multi-nanorods for electrocatalysis to develop next-generation PEFCs.

Acknowledgments

This study was supported by New Energy and Industrial Technology Development Organization (NEDO).

References

[1] N. Zettsu, J.M. McLellan, B. Wiley, Y. Yin, Z.-Y. Li, Y. Xia, Angew. Chem. Int. Ed. 45 (2006) 1288–1292.
[2] M. Shao, T. Yu, J.H. Odell, M. Jin, Y. Xia, Chem. Commun. 47 (2011) 6566–6568.
[3] N. Tian, Z.Y. Zhou, S.G. Sun, Y. Ding, Z.L. Wang, Science 316 (2007) 732–735.
[4] Y. Xiong, Y. Xia, Adv. Mater. 19 (2007) 3385–3391.
[5] L. Zhang, F. Hou, Y. Tan, Chem. Commun. 48 (2012) 7152–7154.
[6] Z. Shen, M. Yamada, M. Miyake, Chem. Commun. (2007) 245–247.
[7] C. Wang, Y. Hou, J. Kim, S. Sun, Angew. Chem. Int. Ed. 46 (2007) 6333–6335.
[8] Z. Zhang, D.A. Blom, Z. Gai, J.R. Thompson, J. Shen, S. Dai, J. Am. Chem. Soc. 125 (2003) 7528–7529.
[9] Z. Zhang, M. Li, Z. Wu, W. Li, Nanotechnology 22 (2011) 015602.
[10] B.J. Wiley, Y. Chen, J.M. McLellan, Y. Xiong, Z.-Y. Li, D. Ginger, Y. Xia, Nano Lett. 7 (2007) 1032–1036.
[11] L.G. Zhou, H. Huang, Phys. Rev. Lett. 101 (2008) 266102.
[12] J.S. Sekhon, S.S. Verma, Plasmonics 7 (2012) 453–459.
[13] Y. Wang, H. Yang, J. Am. Chem. Soc. 127 (2005) 5316–5317.
[14] H. Liu, D. Ma, X. Bao, Dalton. Trans. (2009) 1894–1896.

[15] B. Lim, M. Jiang, P.H. Camargo, E.C. Cho, J. Tao, X. Lu, Y. Zhu, Y. Xia, Science 324 (2009) 1302–1305.
[16] S. Guo, S. Dong, E. Wang, ACS Nano 4 (2009) 547–555.
[17] V.S. Myers, A.I. Frenkel, R.M. Crooks, Langmuir 28 (2012) 1596–1603.
[18] L. Wang, Y. Nemoto, Y. Yamauchi, J. Am. Chem. Soc. 133 (2011) 9674–9677.
[19] M. Wen, Y.-Z. Zhu, Q.-S. Wu, F. Zhang, T. Zhang, J. Phys. Chem. C 113 (2009) 19883–19890.
[20] Y. Xia, Y. Xiong, B. Lim, S.E. Skrabalak, Angew. Chem. Int. Ed. 48 (2009) 60–103.
[21] H.A. Gasteiger, S.S. Kocha, B. Sompalli, F.T. Wagner, Appl. Catal. B Environ. 56 (2005) 9–35.
[22] J. Greeley, I.E.L. Stephens, A.S. Bondarenko, T.P. Johansson, H.A. Hansen, T.F. Jaramillo, J. Rossmeisl, I. Chorkendorff, J.K. Nørskov, Nat. Chem. 1 (2009) 552–556.
[23] A.-X. Yin, X.-Q. Min, W. Zhu, W.-C. Liu, Y.-W. Zhang, C.-H. Yan, Chem. Eur. J. 18 (2012) 777–782.
[24] M.K. Debe, Nature 486 (2012) 43–51.
[25] R. Loukrakpam, P. Chang, J. Luo, B. Fang, D. Mott, I.T. Bae, H.R. Naslund, M.H. Engelhard, C.J. Zhong, Chem. Commun. 46 (2010) 7184–7186.
[26] W. Yang, X. Wang, F. Yang, C. Yang, X. Yang, Adv. Mater. 20 (2008) 2579–2587.
[27] S.-I. Choi, S. Xie, M. Shao, J.H. Odell, N. Lu, H.-C. Peng, L. Protsailo, S. Guerrero, J. Park, X. Xia, J. Wang, M.J. Kim, Y. Xia, Nano Lett. 13 (2013) 3420–3425.
[28] J. Zhang, H. Yang, J. Fang, S. Zou, Nano Lett. 10 (2010) 638–644.
[29] J. Wu, J. Zhang, Z. Peng, S. Yang, F.T. Wagner, H. Yang, J. Am. Chem. Soc. 132 (2010) 4984–4985.
[30] S. Sun, G. Zhang, D. Geng, Y. Chen, R. Li, M. Cai, X. Sun, Angew. Chem. Int. Ed. 50 (2011) 422–426.
[31] C. Koenigsmann, W.P. Zhou, R.R. Adzic, E. Sutter, S.S. Wong, Nano Lett. 10 (2010) 2806–2811.
[32] J. Zhang, J. Ma, Y. Wan, J. Jiang, X.S. Zhao, Mater. Chem. Phys. 132 (2012) 244–247.
[33] B. Fu, W. Liu, Z. Li, Appl. Surf. Sci. 256 (2010) 6899–6907.
[34] Y. Xing, Y. Cai, M.B. Vukmirovic, W.-P. Zhou, H. Karan, J.X. Wang, R.R. Adzic, J. Phys. Chem. Lett. 1 (2010) 3238–3242.
[35] F. Ye, H. Liu, W. Hu, J. Zhong, Y. Chen, H. Cao, J. Yang, Dalton. Trans. 41 (2012) 2898–2903.
[36] H. Zhang, M. Jin, J. Wang, W. Li, P.H. Camargo, M.J. Kim, D. Yang, Z. Xie, Y. Xia, J. Am. Chem. Soc. 133 (2011) 6078–6089.
[37] C. Koenigsmann, A.C. Santulli, K. Gong, M.B. Vukmirovic, W.P. Zhou, E. Sutter, S.S. Wong, R.R. Adzic, J. Am. Chem. Soc. 133 (2011) 9783–9795.
[38] Y.Y. Feng, G.R. Zhang, J.H. Ma, G. Liu, B.Q. Xu, Phys. Chem. Chem. Phys. 13 (2011) 3863–3872.
[39] J. Yang, W. Zhou, C.H. Cheng, J.Y. Lee, Z. Liu, ACS Appl. Mater. Interfaces 2 (2010) 119–126.
[40] M. Shao, A. Peles, K. Shoemaker, Nano Lett. 11 (2011) 3714–3719.